Photocatalytic process in TiO2/graphene hybrid materials. Evidence of charge separation by electron transfer from reduced graphene oxide to TiO2

Photocatalytic process in TiO_2/graphene hybrid materials. Evidence of charge separation by electron transfer from Reduced Graphene Oxide to TiO_2

M. Minella, F. Sordello, C. Minero *

Department of Chemistry and NIS Center of Excellence, University of Torino, Via P. Giuria 5, Torino 10125, Italy, http://www.environmentalchemistry.unito.it.
* Corresponding author. Fax +39-011-6705242; E-mail: claudio.minero@unito.it.

Abstract

Different amounts of graphene oxide were chemically reduced with hydrazine in the presence of nanometric TiO_2 and SiO_2. The photocatalytic performance of the resulting hybrid materials was compared with pristine supports using phenol and methylene blue (MB) under two different irradiation conditions (UV-Vis and Vis only light). MB is strongly adsorbed on the hybrid materials. Significant MB degradation rates were observed on pristine TiO_2 and hybrid TiO_2-reduced graphene oxide (rGO) material under both irradiation conditions. In the presence of the hybrid catalyst, the degradation of MB under Vis is due to the dye-sensitized mechanism, while under UV-Vis there is an additional semiconductor-based photocatalytic mechanism. Conversely, the presence of rGO reduces the rate of photocatalytic transformation for the poorly adsorbed phenol under UV irradiation, and a negligible degradation rate was observed under Vis.

The UV-Vis absorption spectra of aqueous suspensions of hybrid materials with different rGO loading indicate a strong interaction of the two materials and a reduction of the light absorption due to the presence of rGO. Among many mechanisms reported on the role of rGO, it is inferred that the working mechanism involves electron transfer from photoexcited states of rGO onto the titania, and holes migration from titania to rGO, where adsorbed substrates are oxidized. This oxidation is possible only if the substrate HOMO has higher energy (less positive standard redox potential) than the empty states of excited rGO, supposedly for MB and not for phenol. Then, reduced graphene is advantageous when substrates are adsorbed and when the charge separation is possible (coupled with a proper semiconductor like TiO_2). Alone, or coupled with low work function oxides like SiO_2, rGO could be ineffective.

Keywords

Reduced Graphene Oxide; TiO_2-rGO hybrid materials; Visible Sensitization; Charge separation; Photocatalysis

1. Introduction

The study of the semiconductor/electrolyte and semiconductor/gas interfaces has been driven by their potential multisectorial applications [1,2,3,4,5,6]. The main limits to the application of the related technology are: i) the low photonic efficiency of current photocatalysts; ii) the low absorption in the visible spectrum. Crucial issues are the low efficiency in the photogenerated charge carrier separation and the low rate of interfacial charge transfer reactions. [7] Complex strategies have been proposed to increase the performance of semiconductor photocatalysts [8,9,10,11,12,13,14,15,16,17]. More recently, the enhancement of photocatalytic performances has been obtained with nano-hybrid materials made with semiconductors and carbonaceous structures (fullerenes, carbon nanotubes, carbon nanohorns, and graphene). [18,19,20,21]

The interest in the TiO_2-graphene nano-composites is based on the role that the carbonaceous phase plays in the photocatalytic process. Graphene shows exceptional adsorption ability toward various classes of compounds promoting the adsorption of pollutants on the catalyst surface, prerequisite for their efficient photocatalytic removal if and only if the photogenerated charges move toward graphene.

The methods for the graphene production are numerous [22,23,24,25], but the synthesis of non-functionalized graphene does not allow the production of TiO_2-graphene hybrid materials due to the absence of functional groups able to bond to the semiconductor [26,27]. For these reasons the most useful method for the synthesis of TiO_2-graphene photocatalysts is based on the synthesis of graphite oxide by means of chemical oxidation, its exfoliation in water and subsequent reduction of graphene oxide (GO). The final materials are usually defined as reduced GO (rGO), whatever the reduction strategies are, due to the partial preservation of some oxidized moieties in their structure. [28,29]

In the degradation of organic substrate on TiO_2-rGO composites, the main active oxidation species were inferred from the disappearance kinetics of different substrates in the presence of $^{\bullet}OH$ and hole (h_{vb}) scavengers. These experiments demonstrated that the main reactive species are not free hydroxyl radicals and that the direct hole transfer is the main mechanism. [30,31]

Till now a complete agreement on the role of rGO during the photocatalytic process on TiO_2-rGO hybrids has not be reached. The operational mechanisms active on TiO_2-rGO composites as emerges from literature can be summarized as follow.

A. In the case of substrates that do not absorb light and are negligibly adsorbed on catalyst the photodegradation could take place mainly via the “classic” UV-based photocatalytic process promoted by UV-activated band to band transition in which no electron transfer between TiO_2 and rGO is operational and rGO acts only as competitive light absorber, because the GO and rGO electronic structure could preclude any injection of electrons from TiO_2 toward the carbonaceous phase or *vice-versa*. [30]. In addition, the adsorption of carbonaceous phase can generate intraband gap states, located immediately above the VB or below the CB which can extend the absorption of light to the Vis range.
B. When the movement of photogenerated charges from the two phases (TiO_2 and rGO) is not hindered and substrates which do not absorb light are involved, two possible and alternative mechanisms can operate.

1) Electron transfer from rGO to TiO_2. The photocatalytic process is promoted by rGO, which absorbs visible (and UV) photons. Photo-excited electrons in high-energy rGO states are then delocalized (with kinetics in the 0.1-0.2 ps range [32]) onto the TiO_2 structure. Zhang and co-workers demonstrated the role of graphene as a macromolecular photosensitizer instead of an electron reservoir on irradiated rGO-ZnS composites. [33] The time-domain *ab initio* analysis carried out by Long and co-workers [32] highlighted that electron transfer process can occur from photoexcited states of perfect graphene sheets onto the titania surface with a non adiabatic

mechanism. The injected electron located in interfacial states then moves into bulk TiO_2 dissipating the energy *surplus* due to electron-vibrational interactions. [32]

2) Electron transfer from TiO_2 to rGO. A UV-based transaction promotes electrons into the TiO_2 CB which are rapidly transferred onto the graphene-like sheets. The common reaction scheme proposed for the interface rGO/TiO_2 allows the delocalization of TiO_2 CB electrons onto the rGO structure (rGO in this case acts as an electron reservoir). The work function of graphene is 4.42 eV, while the conduction band (CB) of TiO_2 is located at –4.21 eV with energy gap amplitude of 3.2 eV (for the most photoactive anatase allotrope). [34,35,36] As a consequence, the electrons photo-promoted in the CB can be injected into the graphene aromatic structure avoiding their recombination with the valence band (VB) holes. The decrement of the electron transfer resistance at the TiO_2-rGO/electrolyte interface compared to that at the TiO_2/electrolyte interface, observed with EIS by Wang et al., suggested a rapid photoinduced charge separation and a diminished possibility of electron–hole recombination on irradiated TiO_2-rGO materials. [31] Wang et al. proposed that not only electrons can be easily transferred from photo-excited TiO_2 onto rGO sheets, but also valence holes can move toward the rGO phase promoting an effective degradation of adsorbed phenol molecules. [37]

The injection of electrons from excited rGO states toward TiO_2 CB or alternatively from TiO_2 CB toward delocalized empty rGO states is not a sufficient condition to guarantee the degradation of the substrate, because the photogenerated empty states (a hole in the VB or an empty states in the rGO) must be low enough in energy (redox potential sufficiently positive) to promote the oxidation of the substrate itself (injection of an electron from the substrate to the photogenerated empty state). It is worth noting the stability of certain organic substrates under UV irradiated TiO_2 as a consequence of their too low HOMO energetic position (e.g. cyanuric acid is stable in photocatalytic conditions [38,39]). Consequently, the energetic position of the HOMO of a substrate is a key point to allow its transformation under irradiated TiO_2-rGO hybrids especially in the case of Vis only irradiation which does not activate TiO_2 band to band transitions which generate very oxidant VB holes.

C. In the presence of dyes, other two different visible-activated dye-sensitized pathways have to be considered: in the case of a pure TiO_2 catalyst the adsorbed dyes can inject photo-excited electrons onto the titania CB, while in the presence of TiO_2-rGO composites this mechanism can couple with an alternative reaction path in which the dye photo-excited electrons can be delocalized in the electronic diffuse states of rGO. In both cases the oxidized dye molecules, formed as a consequence of a single or multi-electron injection from the photo-excited dye to the delocalized empty states of rGO or TiO_2, can autonomously evolve toward transients or stable by-products and consequently toward the substrate degradation. Pastrana-Martínez et al. from an in depth analysis of the photocatalytic activity of TiO_2-rGO composites toward the colorless diphenhydramine and the organic dye methyl orange, emphasized the complexity of the operational mechanisms concluding that rGO can operate as visible light sensitizer of TiO_2, but in the presence of visible-absorbing species the degradation process can be dominated by a direct self-oxidation of the visible-absorbing species. [30]

Herein, we report the two-steps synthesis of TiO_2-rGO hybrid materials (synthesis of GO by chemical oxidation of graphite, exfoliation and in situ reduction of GO on the TiO_2 surface) and the investigation of their photocatalytic behavior. The photocatalytic tests were carried out comparing two substrates and two illumination sources aiming to give insight on the working mechanisms and on the relation between the absorbing optical properties of the tested catalyst and its photocatalytic behavior. This approach allows us to discriminate among the potential

operational photocatalytic mechanisms cited above and, hopefully, to clarify some aspects of the photo-reactivity of TiO_2-rGO composites.

2. Materials and Methods

2.1 Materials

Graphite natural powder (briquetting grade, ≈ 100 mesh, 99.9995%) was purchased from Alfa Aesar, H_3PO_4 (85%), H_2SO_4 (96%), $KMnO_4$ (>99%), HCl (37%), methanol gradient grade from Carlo Erba and $HClO_4$ (85%), Methylene Blue (MB) trihydrate (>99%), H_2O_2 (35%), hydrazine monohydrate (98%) and phenol (>99%) from Sigma Aldrich. Titanium dioxide (Hombikat N100: 100% anatase, BET specific surface area 100 m^2/g, average crystal size 20 nm) was purchased from Sachtleben Pigments. Fumed silica SiO_2 Aerosil OX 50 (BET specific surface area 50 $m^2\ g^{-1}$) was bought from Evonik. Zero-grade air for Total Organic Carbon (TOC) analysis was purchased from Sapio (Turin, Italy). All the compounds were used as received without any further purification step. Water was purified with a MilliQ plus apparatus (in-line TOC = 2 ppb, conductivity 18.2 MΩ cm, Merck Millipore).

2.2 Synthesis of GO and TiO_2-rGO hybrid materials

Graphene oxide was produced by chemical oxidation using the modified Hummers and Staudemaier's method [40] proposed by Huang et al. [41]. Briefly, 500 mg of graphite powder were dispersed in a solution obtained with 27.3 mL H_2SO_4, 3.30 mL H_3PO_4 and 2.78 g $KMnO_4$. The suspension was magnetically stirred at r.t. for 1, 2 or 3 days, respectively. After 12-15 hours a viscous brownish gel was obtained. After the desired oxidation time the suspension was carefully diluted in 120 mL of water and titrated with H_2O_2 till a bright yellow suspension was obtained (the violet MnO_4^- ions are completely reduced to colorless Mn^{+2}). The yellow graphite oxide formed was washed three times with 1 M HCl and the solid separated with centrifugation (1200 G). During the washing procedure the color changed from bright yellow to brownish. The solid was then washed 3 times with water. During the washing procedure the graphite oxide experienced exfoliation. The suspension was then dialyzed toward water (Spectra/Por® Dialysis Membrane, MW cut off 6-8000 Da) until the pH of the external solution was stable and close to 4. The concentration of carbon in the GO suspensions was evaluated measuring the TOC on diluted suspensions after dialysis.

The TiO_2-rGO hybrid materials were obtained by chemical reduction with hydrazine solution (65 %) of different amounts of GO (3 days of oxidation) in the presence of TiO_2 according to a modification of the method reported in [42]. Stable suspensions of 4 g dm^{-3} TiO_2 in water were obtained by sonication. Different amounts of GO were added to obtain materials with different carbon loading. The addition of GO quickly destabilized the TiO_2 colloids owing to adsorption of GO on the titania surface. Then 300 μL of hydrazine were added drop wise at r.t. After 12 hours of vigorous stirring the suspensions were filtered on 0.45 μm hydrophilic filters (Whatman, NL 17 membrane filters, polyamide) and washed with water. Finally, the produced powder was dried at 373 K for 1 hour.

By using the same method adopted for the synthesis of TiO_2-rGO materials, we produced hybrid SiO_2-rGO materials with different loading of rGO. GO was adsorbed on fumed silica SiO_2 Aerosil OX 50 and reduced with hydrazine. The synthesis of these hybrid materials was aimed to study the photochemical behavior of the rGO adsorbed on an inert support. The low work function of SiO_2 ($\chi \approx 1.2$ eV [43]) hinders the injection of electrons from the excited states of rGO to the inorganic support allowing the study of the photochemical behavior of rGO alone.

2.3 Photocatalytic Tests

The photodegradation experiments were carried out using cylindrical Pyrex cells (4.0 cm diameter and 2.5 cm height, cut-off at 295 nm) on 5 cm^3 of aqueous suspension containing the desired amount of the photocatalyst powder (C_{cat} 0.5 g dm^{-3}), substrate (1 mM phenol or 4×10^{-5} M MB) and $HClO_4$ 10^{-3} M to execute the test at pH 3±0.2. The slurries containing the photocatalyst were prepared using sonication. The irradiation was carried out with a set of three TLK 40W/05 (UV-Vis) or TLK 40W/03 (Vis only) fluorescent lamps (Phillips, Eindhoven, Nederland). The former has an integrated irradiance of 25.2±1 W m^{-2} in the 300-400 nm wavelength range, with a maximum emission at 365 nm (able to activate the band to band transition in TiO_2 based materials), and minor emission in the Vis range (10.5±1 W m^{-2} in the 400-800 nm range). The latter has an integrated irradiance of 40±1 W m^{-2} in the 400-800 nm wavelength range, with a maximum emission at 423-436 nm, and negligible emission in the UV range (1.5 W m^{-2} in the 300-400 nm range). The emission spectra are reported in Fig.1A of the Supplementary Materials (hereafter SM).

During irradiation the suspension was magnetically stirred and the cell temperature was 30±3 °C. After irradiation the suspension was filtered through 0.45 μm cellulose acetate membrane filter (Millipore HA) and analysed as required (HPLC-UV for phenol, spectrophotometrically at 665 nm for MB).

The photocatalytic transformation of the studied substrates followed pseudo-first order kinetics. The profiles of concentrations of the phenol and MB were fitted with a pseudo-first order equation of the form $C_t / C_0 = \exp(-k\, t_{irr})$, where C_t is the substrate concentration at the irradiation time t_{irr}, C_0 the initial concentration, and k the pseudo-first order degradation rate constant. The values of k are reported with their uncertainty (confidence intervals evaluated through the goodness of the fit, representing intra-series variability at 0.95 level of confidence).

2.4 Methods

The extinction spectra of TiO_2, TiO_2-rGO, SiO_2 and SiO_2-rGO suspensions were recorded with a Varian CARY 100 Scan UV-Vis spectrophotometer, using quartz cuvettes with a path length of 1 cm. The % reflectance spectra were recorded on opaque homogenized powdered samples with a Varian Cary 5000 UV-VIS-NIR reflectance spectrometer.

The UV-Vis lamp irradiances were measured with an Ocean Optics USB2000+UV-VIS equipped with a 400 μm optical fiber (30 cm length) with a cosine corrector (Ocean Optics, CC-3-UV-T, optical diffuser in PTFE, wavelength range 200-2500 nm, OD diameter 6.35 mm, Field of View 180°). The spectrometer was calibrated with an Ocean Optics DH-2000-CAL Deuterium-Halogen Light Sources for the UV-Vis-NIR calibrated for absolute irradiance measurements from the vendor (Radiometric Calibration Standard UV-NIR, certificate of calibration #2162).

Phenol degradation kinetic was monitored with HPLC-UV (Hitachi L2200, LaChrom Elite, Lichrospher R100-CH 18/2 column (250 mm)). The elution was carried out at 1 cm^3 min^{-1} with H_3PO_4 4.2 mM: Methanol 85:15 in isocratic mode. The retention time of phenol under this condition is 9.9 minutes. The injection volume was 60 μL.

The measurement of TOC was carried out with a Shimadzu TOC-VCSH Total Organic Carbon Analyzer, equipped with an ASI-V autosampler and fed with zero-grade air. Each suspension of GO, as synthesized, was diluted 200 times with MQ water and analyzed. TOC was obtained from the difference between Total Carbon (TC) and Inorganic Carbon (IC).

The morphology of the hybrid samples before (TiO_2-GO) and after the reduction with hydrazine (TiO_2-rGO) was investigated by means of a high-resolution transmission electron microscope (HR-TEM, JEOL JEM 3010), equipped with a LaB_6 source with an accelerating voltage of 300 kV.

The XPS analysis was carried to investigate the nature of the carbon atoms in the TiO_2-GO and TiO_2-rGO samples. The XPS spectra were recorded on pelletized samples with a VSW TA10 Mg Kα X-ray source (1253.6 eV) equipped with a VSW Class 100 Concentric Hemispherical Analyzer (VSW Scientific Instruments Ltd).

3 Results and Discussion

3.1 Material characterization

The simple oxidation method here adopted allows the preparation of significant amount of GO, the raw material for the successive synthesis of rGO, contrariwise to the sonochemical methods adopted for the exfoliation of graphite and one-step production of micro-amount of graphene nanosheets. [23,44,45]

Fig. 1 shows the UV-Vis absorption spectra of the suspensions of GO obtained after 1, 2 and 3 days of chemical oxidation, respectively. The spectra are normalized for the TOC concentration of the analyzed suspensions. The spectra are dominated by the peaks at ≈230 nm. These signals are due to the $\pi \rightarrow \pi^*$ transition of the C=C bonding. [41,46,47] The accurate position of the peaks are 231, 229 and 228 nm for the samples oxidized for 1, 2 and 3 days (*1D*, *2Ds*, *3Ds*), respectively. The lower is the peak position (as wavelength) the lower is the degree of aromaticity of the graphene-like planar structure. Accordingly, the *3Ds* sample shows the peak at the shortest wavelength. The main peaks has a shoulder at roughly 300 nm, due to the $n \rightarrow \pi^*$ transition of the carbonyl groups. [48,49] The larger is the intensity of the 300 nm shoulder, the larger is the concentration of C=O (carbonyl or carboxyl) groups in the samples and so the degree of oxidation. The ratio between the absorbance at 230 and 300 nm is also informative. This ratio is 2.4, 2.6 and 2.8 for the *1D*, *2Ds* and *3Ds* samples, respectively. It increases with the increment of the oxidation degree because superior is the oxidation of graphene basal planes, greater it is the amount of isolated aromatic rings which increment the absorbance at 230 nm [49]. The obtained ratios (> 2) are very similar to those reported by Huang et al. [41] for GO samples with significantly larger lateral size.

The size of the GO particles after three days of oxidation in the same condition above described has been previously measured with dynamic light scattering (DLS) and reported in [29]. After exfoliation the GO particles have a hydrodynamic radius equal to 500 ± 70 nm. This value is in agreement with those reported by other authors for GO obtained in very similar experimental conditions [50].

The proposed methods for the reduction of GO to graphene are numerous (thermal annealing, microwave and photo reduction [29], chemical, photocatalytic and solvothermal reduction) and affect the final performance of materials. For a full analysis of this topic please refer to the review by Pei and Cheng [51]. The production of the TiO_2-rGO was here carried out by chemical reduction of different amount of GO (*3Ds*) adsorbed on the TiO_2 surface with aqueous hydrazine solution. Different materials with increasing amount of carbon loading (from 0.5 to 5% w/w) were successfully synthesized. The chemical reduction in water by hydrazine and its derivatives results in agglomerated graphene-based nanosheets due to the increase of hydrophobicity. [37] We carried out the reduction of GO adsorbed on TiO_2 at r.t. and at the boiling point. We observed that only in the former case is a single solid phase synthesized, while in the latter case two separated phases are produced. Gao et al. [49] studied systematically the reduction of GO by hydrazine at r.t. and at high temperature. The hydrazine reduction at r.t. completely reduces the epoxide and hydroxyl groups located at the interior of the aromatic domains and only partially the carboxyl moieties at the edge of the aromatic domains. At higher temperature the reduction of the hydroxyls at the edge of the aromatic domains and of the carboxyl groups occurs. [49] Our experimental results support the conclusion that heating allows further reduction of the

oxygenated groups which links GO to the TiO_2 surface (e.g. the ester groups obtained from the reaction between the TiO_2 hydroxyls and the carboxyls of GO). Furthermore, the increment of the hydrophobicity of rGO at higher reduction temperature hinders the interaction between rGO and the hydrophilic TiO_2 surface causing phase separation. Thus, the materials used for the photocatalytic tests are those obtained by reduction at r.t. only.

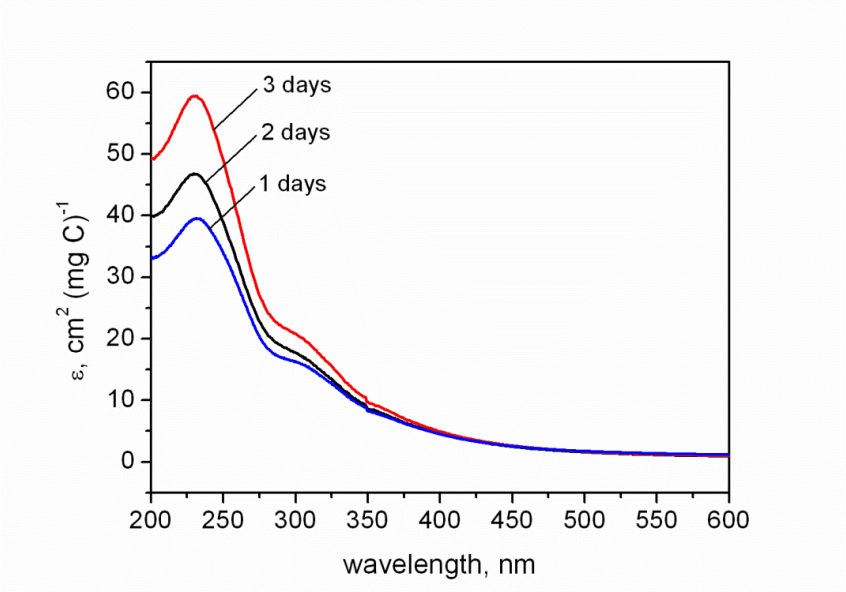

Fig. 1 Absorption spectra of graphene oxide colloid (GO) obtained after different oxidation times (1, 2 and 3 days). The measured absorbance is normalized for the total organic concentration (TOC) of each measured solution.

Fig. 2-SM and Fig. 3-SM show the HR-TEM micrographs of TiO_2-GO and TiO_2-rGO (both with a 5% carbon loading) at different magnifications. No significant differences were observed before and after the chemical reduction of GO with hydrazine at room temperature. The anatase nanoparticles have an average particle size of ≈20 nm and are dispersed on the 2D layers of the graphene structure, which in some cases enfold the TiO_2 nanoparticles.

The effective reduction with aqueous hydrazine of the GO to rGO was evaluated with XPS-ESCA. Fig. 4-SM shows the spectra of the TiO_2-GO and TiO_2-rGO (both with a 5% carbon loading) in the C(1s) core level peak region. The spectrum of TiO_2-GO is dominated by three main overlapped peaks. The peak centered at ≈ 285 eV is related to carbon atoms in sp2 hybridization typical of graphitic/graphenic structures, while the components at higher binding energy (BE at ≈ 287 and 289 eV) can be attributed to carbon species in higher oxidation state. [52,53 and references therein]. In the case of the reduced sample one peak dominates the spectra (BE at ≈ 285), concurrently with a strong suppression of signals for high C-oxidation state. From the comparison of the two spectra (Fig. 4-SM a and b) it is manifest the effective reduction of the carbonaceous phase was obtained with hydrazine.

Fig. 5-SM shows the diffuse Reflectance spectra of the produced TiO_2-rGO materials in the 200-800 nm range, as *%R* and as Kubelka-Munk (K-M) function (eq. 1, left). The rGO phase induces the improved light absorption in the Vis range in line with data previously reported for TiO_2-rGO hybrid materials. [54,55,56] The energy band gap values of the synthesized materials were evaluated from the K-M functions by considering the relation which links the ratio between the absorption and scattering coefficients and the photon energy for semiconductors with indirect band gap, e.g. TiO_2 (eq. 1, right).

$$f(R) = \frac{(1-R_\infty)^2}{2R_\infty} = A(h\nu - E_g)^2 \qquad \text{eq. 1}$$

where *f(R)* is the K-M function, R_∞ the diffuse reflectance approaching infinite sample thickness, *hv* the photon energy, E_g the energy gap and *A* is a constant.

A slight decrement of the apparent E_g values (from 3.28 to 3.20 eV, corresponding to a red shift from 378 to 387 nm, see the inset of Fig. 5B-SM) was observed with the increase of the rGO loading. This can be a consequence of the production of a limited number of localized intraband gap states or simply an apparent band gap due to the superposition of absorption spectra of two different materials. However the slight decrement of the E_g we observed is negligible if compared to that reported for other TiO_2-carbon phase (graphene, carbon nanotubes) hybrid materials. [55,57,58]

The extinction spectra of water suspensions of the studied catalysts at different concentration (10, 50 and 100 mg dm^{-3}) were recorded and the average extinction coefficient $\varepsilon_{ext}(\lambda)$ (Fig. 2A) computed from the plot of absorbance vs concentration, according to the Beer-Lambert law. The linear fits have $r > 0.998$ for all the wavelengths. The analysis of the $\varepsilon_{ext}(\lambda)$ values (sum of the absorption, ε_{abs}, and scattering, ε_{scat}, coefficients) reveals that the increment of the rGO loading decreases the intrinsic ability of catalyst suspensions to absorb the radiation in the whole wavelength range, and consequently the overall amount of photons able to activate the UV-based photocatalytic mechanism is diminished. In addition the spectrum of hybrid materials suggests that there is strong interaction between TiO_2 and rGO, as the ratio of typical UV absorption bands of TiO_2 is changed (see bands at 273 and 323 nm, respectively). Moreover a large extinction (absorption + scattering) is present in the Vis range.

Fig. 2B shows the extinction spectra of water suspensions of nanometric silica (average size 40 nm) and of the composite SiO_2-rGO with 1% of carbon loading. The addition of rGO slightly increases the extinction. The spectrum of the SiO_2 colloid, because of the high band gap of silica (8.9 eV [59]), is dominated by the contribution of Mie-scattering only. The SiO_2-rGO colloid retains the scattering profile of silica, overlapped with an almost flat absorption of rGO till 240 nm. Conversely, the rGO loading on TiO_2, which has similar surface hydrophilicity of SiO_2, reduces the UV-Vis extinction and totally changes the absorption spectrum, indicating a strong interaction between rGO and the semiconductor electronic structure. The absorption peak of rGO below 240 nm (Fig. 2B) is also manifest in the spectra of TiO_2-rGO colloids at $\lambda < 240$ nm (Fig. 2A), where this peak overlaps with the complex profile resulting from the scattering and absorption properties of TiO_2 strongly modified by the interaction with rGO.

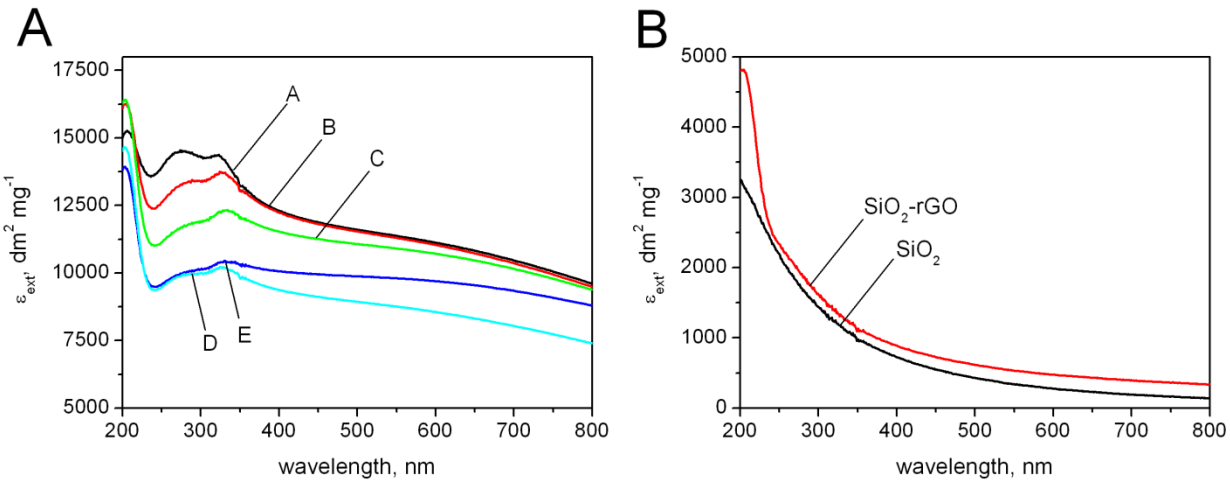

Fig. 2 Extinction coefficient (ε_{ext}) of water suspensions of A) TiO_2-rGO hybrid materials with different % rGO: A= 0 %; B= 0.5 %; C= 1.0 %; D= 2.5 %; E= 5.0 %; B) SiO_2 and SiO_2-rGO (1 % of rGO) The values of ε_{ext} were obtained from the extinction spectra of suspensions with concentrations equal to 10, 50 and 100 mg dm^{-3} of the hybrid material.

3.2 Photocatalytic experiments

The photocatalytic performance of the synthesized photocatalysts was evaluated using two different compounds, phenol and MB, under UV-Vis (TLK 40W 05 lamp) and Vis only irradiation (TLK 40W 03 lamp). The absorption spectra of phenol and MB in water solution are reported in Fig.1B-SM. The comparison of lamp emission spectra and substrate absorption spectra (Fig. 1-SM) shows that phenol does not absorb with both lamps, whilst MB absorbs from both lamps the two emission peaks in the 540-580 nm range and from the TLK03 (Vis spectrum) absorbs in the 420-480 nm range in its peak tail.

The MB spectrum in solution changes when MB is adsorbed. Fig. 3 reports reflectance spectra of MB adsorbed on pristine TiO_2 and the MB adsorbed as a function of the solution concentration (KM function, inset of Fig. 3). To measure the spectra, definite amounts of pristine TiO_2 were equilibrated in the dark in the presence of increasing amount of MB (0 to 8.0×10^{-5} mol/g TiO_2). After equilibration the suspensions were filtered and dried in oven at 373 K for 1 hour. The dried powders were grinded and their %R spectra were recorded. As Fig. 3 reports, the quantity adsorbed is linear with MB solution concentration, indicating that at 8.0×10^{-5} mol g^{-1} on pristine TiO_2 the surface is far from saturation of the MB adsorbing sites. The same ratio $[MB]/C_{TiO2}$ will be used during the photodegradation experiments. From reflectance spectra of Fig. 3 it is also manifest a blue shift of ≈ 80 nm for the MB absorption maximum. This shift is comparable to that reported in the literature [60,61,62] for the formation of MB dimers. Because the significant adsorption of MB onto the TiO_2 surface, the blue shift can be ascribed to adsorption on TiO_2 surface. A shift of ≈ 80 nm of the absorption maximum corresponds to a transition between two states separated by 0.24 eV in energy, and an equilibrium adsorption constant of roughly 1.2×10^4, slightly larger than the reported values ($3–10\times10^3$) for dimerization in solution [60,61,62]. The strong interaction of MB with the catalyst surface is an essential condition for an efficient electron transfer in the case of correct positioning of the energy bands/states. This shift increases the absorption of adsorbed MB in the presence of TLK03 (Vis spectrum), whilst it has only a minor effect on absorption in the case of illumination with the TLK05 (UV spectrum).

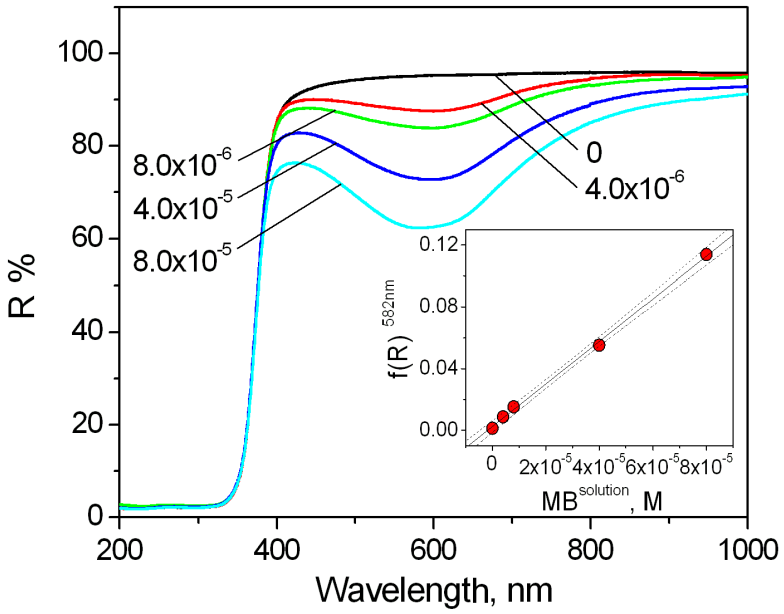

Fig. 3 % Reflectance spectra of TiO_2 Hombikat N100 equilibrated in the presence of different amount of MB (mol MB / g TiO_2 from 0 to 8.0×10^{-5} mol/g). Inset: K-M function value at 582 nm ($f(R)^{582nm}$) for the samples equilibrated at different concentrations of MB in solution.

3.2.1 Phenol

Fig. 4 shows the photocatalytic time evolution under UV-Vis light of phenol in the presence of TiO_2-rGO, with different rGO loading at total catalyst concentration C_{cat} = 0.5 g dm^{-3}. The degradations follow first order kinetics. The degradation kinetic constants are reported in the inset of Fig. 4 and in Table 1-SM (entries 1-5). The phenol degradation rate decreases with the increment of the rGO loading. Opposite to the reported data, where the coexistence of rGO and TiO_2 phases induced generally better photocatalytic performances [21,37], in this case the presence of rGO decreases the substrate transformation rate. Under the adopted experimental conditions the amount of phenol adsorbed on TiO_2 is negligible compared to the fraction remaining in solution, and in the presence of increasing amount of rGO no increment of the adsorbed fraction of phenol was observed. This evidence is contrasting with data reported by Wang et al. [37] who observed an increment of the adsorbed phenol fraction with the increment of %rGO on TiO_2-rGO composites synthesized by a one-step hydrothermal method. The different results could be related to the different synthetic procedure, which could give materials with a significantly different degree of rGO reduction.

As under UV-Vis irradiation only the catalyst absorbs light, the decrease of phenol degradation rate with increasing rGO loading depends on the reduction of extinction spectra as % rGO increases, as already discussed with reference to Fig. 2. Factually, less light is absorbed, leading to a reduced charge carrier production and the decrease of the rate. A competition for UV light between the inorganic and rGO phase was also recently proposed by Xiong et al. [63] to justify the experimental evidences observed with $BiOIO_3$-rGO nanocomposites under Vis and UV irradiation. From spectra in Fig. 2 it is not possible to decouple absorption and scattering processes, although reflectance spectra in Fig. 5-SM suggest that absorption is mainly due to band-gap absorption of TiO_2. Then the visible tail observed in Fig. 2 is due only to scattering properties of N100 TiO_2. In the presence of rGO, less light is absorbed by TiO_2 because of the presence of the adsorbed rGO phase increases the scattering over the entire UV-Vis spectrum. Alternatively, a lowering of the quantum yield due to a larger recombination rate due to an increasing amount of rGO on TiO_2 can be invoked. In this case instead of being beneficial, rGO would behave as a recombination center. This would happen independently on the substrate, contrary to many positive effects reported in literature and later in this work. Consequently, this last hypothesis is discarded.

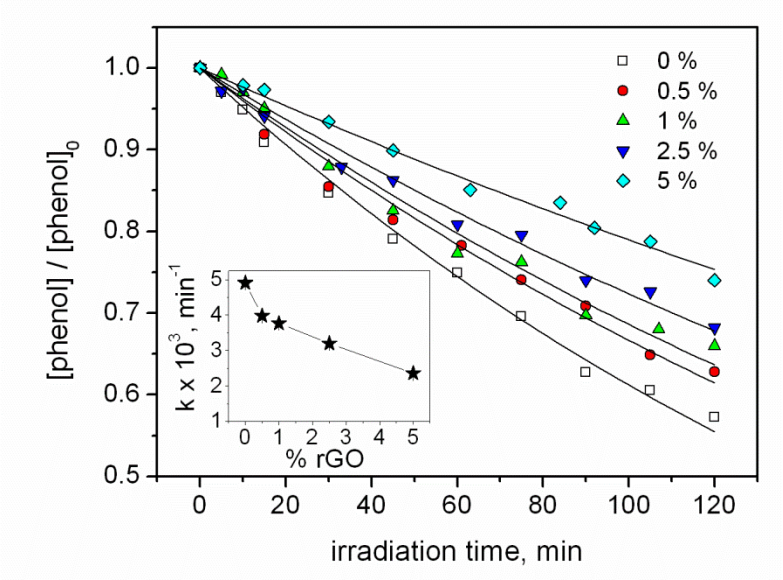

Fig. 4 Photocatalytic degradation under UV irradiation (TLK 40W 05) of 1 mM phenol at pH 3 on TiO_2-rGO hybrid materials with different rGO loading. C_{cat} 0.5 g dm^{-3}. Inset: pseudo first order kinetic constants for the photocatalytic transformation of phenol as a function of the % rGO.

Phenol degradation was also carried out under Vis light (TLK 40W 03 lamp). Very low degradation rates were observed in the presence of both pristine TiO_2 and TiO_2-rGO materials. The kinetic constant observed for TiO_2-2.5% rGO was $(1.9\pm0.1)\times10^{-4}$ min^{-1}, 17 times lower than the degradation kinetic constant measured under UV irradiation. These results indicate that the absorption of the hybrid photocatalyst, and mainly of rGO, as pristine TiO_2 is not excited in the Vis, does not produce photoexcited species able to carry out the reaction with phenol. The possible hypotheses are two: 1) the excited rGO is not able to inject electrons in TiO_2, and photogenerated species recombine in rGO very rapidly compared to their reaction rate with phenol; 2) The excited electrons in high energetic rGO states can be delocalized toward TiO_2 conduction band (rGO injects electrons into TiO_2), charge separation is attained and photogenerated species do not recombine, but HOMO of the substrate to be transformed (here phenol) is lower in energy than the energy state of rGO where an electron vacancy has been photogenerated. In this case the reaction is thermodynamically impeded. However it is possible that with other substrates this thermodynamic impediment is removed. As an example, in the case of risperidone, which does not absorb in near UV-Vis, the loading of rGO on TiO_2 increases the photocatalytic rate both under near UV and Vis irradiation.[64]

3.2.2 Methylene Blue

Fig. 5A shows the change in the MB concentration under UV-Vis irradiation. The dye concentration in solution before the irradiation is lower than the nominal value in every instance in agreement with the adsorption discussed before (see also Fig. 3) . The adsorption of MB in the adopted conditions is significant and increases with the increment of the rGO loading (e.g. TiO_2-5%rGO adsorbs more than 85 % of the added MB, see inset of Fig. 5A).

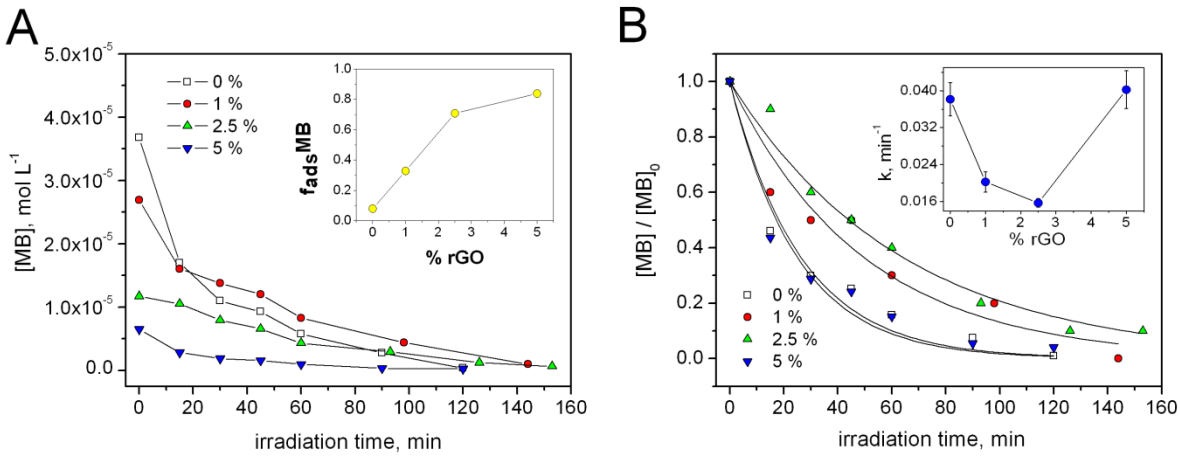

Fig. 5 Photocatalytic degradation under UV-Vis of $4x10^{-5}$ M of MB at pH 3 in the presence of TiO_2-rGO with different % rGO. C_{cat} 0.5 g dm^{-3}. MB concentration (A) and fraction of MB (B) in solution as a function of the irradiation time. Insets: (A) fraction of MB adsorbed on the catalyst as a function of the % rGO; (B) pseudo first order kinetic constants for the MB transformation as a function of the % rGO.

The C/C_0 showed exponential decay (Fig. 5B). The overall observed kinetic constants k_{obs} are reported as inset in Fig. 5B and in entries 6-9 of Table 1-SM. The observed kinetic constants are deduced from the time evolution of [MB] in aqueous solution as $d[MB_{sol}]/dt=-k_{obs}\times[MB_{sol}]$. The linear relation of $[MB]_{ads}$ vs $[MB]_{sol}$ evidenced in Fig. 3 suggests that $[MB]_{ads} = \beta\ \phi\ C_{cat}\ K\ [MB]_{sol}$, where β is the moles of sites per catalyst mass, ϕ is the fraction of constituent of the hybrid catalyst, C_{cat} is the mass dm^{-3} of hybrid catalyst, and K is the equilibrium adsorption constant. In the case of linear partition between the aqueous phase and rGO / TiO_2 phases, it can be demonstrated that $k_{obs}=k_{tot}$, where k_{tot} is the first order kinetic constant that would be obtained following the time evolution of the total concentration in the system (both adsorbed and free)

from $d[MB_{tot}]/dt=-k_{tot}\times[MB_{tot}]$. In other cases they are proportional. Then, the trend of observed kinetic constants k are representative of the overall degradation of substrate in the hybrid system. The rate equations that can be derived from a kinetic model by taking into account the adsorption constants and kinetic constants specific for the two adsorbing phases (k_G and k_T, for rGO and TiO_2, respectively), are not developed here as they are outside of the scope of the paper. However, assuming that the rate at the surface is proportional to the local (adsorbed) concentration it can be easily demonstrated that there is no minimum or maximum of k_{obs} as a function of the rGO amount. When $k_G>k_T$, the rate increases with graphene content and vice versa, irrespective of the value of the adsorption constants. Then the observed effects must be explained with factors other than those above cited (adsorption constants and kinetic constants specific for the two adsorbing phases).

As observed for the UV photocatalytic abatement of phenol, also in this case the presence of rGO has an initial negative effect. The kinetic constants show a minimum for 2.5% rGO. This is conflicting with the previously reported bell-shaped profile of the rate with the increment of %rGO. [31] The discrepancies point out the role of the method of synthesis which can significantly affect the properties of the material and consequently its photocatalytic behavior. The observed dependence of the rate on the rGO amount can be explained invoking two different effects. At low rGO loading the shielding of TiO_2, as already discussed for phenol, decreases the light absorbed by TiO_2. In addition, assuming that the reactivity is mainly dominated by TiO_2, a stronger adsorption on graphene than on TiO_2 implies that the substrate is scarcely transferred during the photocatalytic reaction to the TiO_2 surface. It is apparent that because the substrate is adsorbed on graphene, it must react on its surface. Consequently, due to the two cited reasons the overall reaction rate will be reduced unless holes on TiO_2 (already decreased by light shielding) are transferred to rGO. As a further increase of rGO loading increases both the MB adsorbed on rGO and the rate, it must definitely concluded that MB reacts on rGO and transfer of holes from TiO_2 to rGO is operating. This conclusion agrees with Wang et al. [31] that holes are the main oxidant species and that in the hybrid catalyst oxidative species are not changed by introduction of graphene-like carbon to TiO_2. Concurrently with TiO_2 excitation, also rGO absorbs light and excited electrons in high energetic rGO states must be delocalized toward TiO_2 conduction band (rGO injects electrons into TiO_2) to avoid recombination.

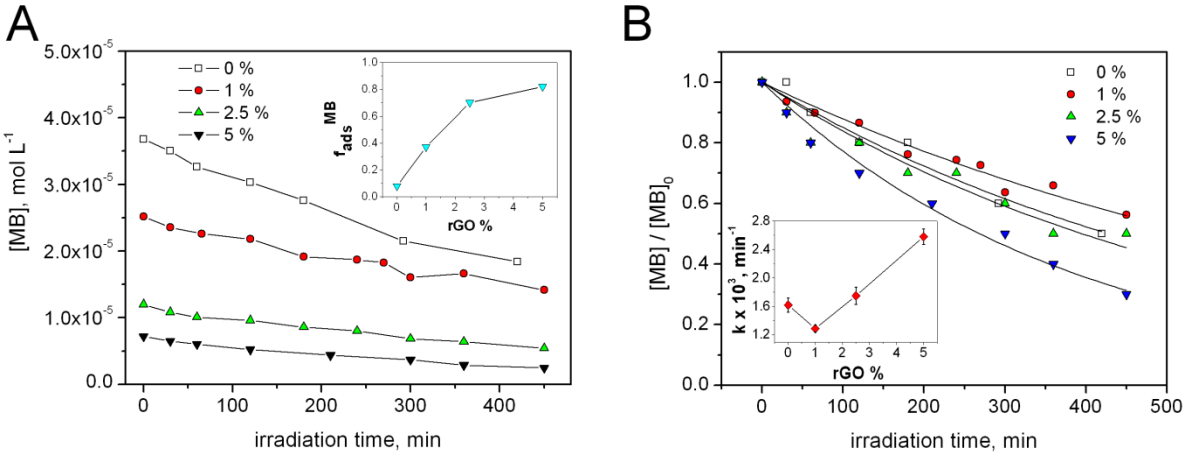

Fig. 6 Photocatalytic degradation under Vis irradiation of $4x10^{-5}$ M of MB at pH 3 in the presence of TiO_2-rGO with different % rGO. C_{cat} 0.5 g dm^{-3}. MB concentration (A) and fraction of MB (B) in solution as a function of the irradiation time. Insets: (A) fraction of MB adsorbed on the catalyst as a function of the % rGO; (B) pseudo first order kinetic constants for the MB transformation as a function of the % rGO.

Fig. 6A and Fig. 6B show the change in the MB concentration in solution under Vis irradiation and the related C/C_0 profiles. The amount of MB adsorbed in this experiment (inset of Fig. 6A)

is quite similar to that observed for previous experiments (inset of Fig. 5A), so a strong adsorption of MB with increasing rGO loading is confirmed. Opposite to the case of phenol photocatalytic degradation under Vis irradiation where negligible removal of the substrate was detected, in this case the MB disappearance is significant, although at irradiation times longer than under UV-Vis irradiation. The abatement profiles follow an exponential decay and the overall *k* kinetic constants are reported in the inset of Fig. 6B (and entries 10-13 of Table 1-SM).

The kinetic constants, after a minimum for TiO_2-1%rGO, increase with the increment of the %rGO, with a shape similar to that observed under UV-Vis irradiation, but with values lower of about one order of magnitude. Under Vis irradiation both rGO and MB can absorb, whilst TiO_2 does (almost) not. The slight decrease of the rate at TiO_2-1%rGO could be due to the previous invoked effect of light shielding on TiO_2, as also with the Vis lamp a small absorption by TiO_2 is still possible and a minimal contribution of semiconductor mechanism is present. So the degradation mechanism must involve the light absorption by rGO, or a dye sensitized mechanism.

Between the two hypotheses made for justifying the very scarce reactivity of phenol, the first one (fast recombination of photogenerated species in rGO because the excited rGO is not able to inject electrons into TiO_2) must be rejected as MB transforms. The second hypothesis (rGO injects electrons into TiO_2) could be fine if the HOMO of MB is higher in energy than the energy state of rGO where an electron vacancy has been photogenerated. In this case the reaction is thermodynamically favored and charge separation is attained. However, the increase of rGO content implies that the amount of absorbed light is reduced (see Fig. 2A) and consequently the rate would be diminished, contrary to what is observed (inset of Fig. 6B). Then, the MB degradation must be explained by considering a dye-sensitized mechanism.

The dye-sensitized mechanism involves the light absorption by MB, charge injection into TiO_2 or rGO and evolution of the oxidized MB to products. The absorption of light from the MB-TiO_2 surface species was well studied [21,65,66] and the role of self-induced photosensitization outlined.[67] The excited electrons, which occupy the LUMO of the adsorbed MB on TiO_2, can be injected into titania CB promoting the MB degradation. As MB is adsorbed on TiO_2 (Fig. 3) but preferentially adsorbed on rGO (insets of Fig. 5A and Fig. 6A), the electron must be injected from the LUMO of MB to rGO. Then, according to the conclusions drawn from MB irradiation under UV-Vis lamp, rGO would transfer these electrons to TiO_2.

To confirm these conclusions, experiments of MB photodegradation under Vis irradiation was carried out in the presence of the SiO_2-rGO hybrid materials synthesized by using the same methods adopted for producing TiO_2-rGO. Under the adopted experimental conditions (0.5 g dm^{-3} of catalyst, initial MB concentration $4x10^{-5}$ M, pH 3), the silica adsorbs a significant amount of MB (around 75%) and this value increases with the increment of the % rGO. Both on pristine SiO_2 and on SiO_2-rGO hybrid materials, no MB photocatalytic degradation was observed under the adopted conditions. From an energetic point of view an electron in the LUMO of MB adsorbed on the catalyst surface (SiO_2 or SiO_2-rGO) is not able to move toward the CB of SiO_2. This conclusion was expected for SiO_2 due to its very high work function [43]. Then on SiO_2 after light excitation of MB only recombination is possible. In the presence of rGO, as reaction does not proceed and also electron transfer from rGO to SiO_2 is impeded because of the SiO_2 high work function, the electron transfer to empty electronic states of rGO must be followed by recombination with oxidized MB, giving a null cycle.

Then the mechanism of MB degradation in the presence of the hybrid TiO_2-rGO is initially promoted by a dye-sensitized mechanism. In the presence of rGO, electrons are mostly transferred to rGO, and then from rGO to TiO_2. When excited electrons in rGO cannot be released (for example to TiO_2, for which rGO acts as sensitizer and also as hole acceptor), rGO acts a recombination center.

4. Conclusions

The analysis of the photocatalytic behavior of TiO_2-rGO hybrid materials synthesized at different loading of rGO, underlines its complexity as the working mechanisms depend not only on the substrate degraded, but also on the kind of irradiation adopted. A careful optical characterization of the hybrid materials and lamp emission allows disentangling many tricky rate trends observed changing % rGO in the hybrid catalyst. Phenol is degraded predominantly via UV-based photocatalysis and the content of rGO decreases the rate by increasing the amount of scattered light. MB is degraded via UV-based photocatalysis and in the case of visible irradiation via a dye-sensitized mechanism. Visible sensitization driven by rGO phase seems not to be the predominant mechanism in the studied experimental conditions and with the studied photocatalytic materials. However, rGO plays a key role for adsorption and as electron passageway for dye-sensitized mechanism. Because the adsorption of MB on the TiO_2 surfaces activates the dye-sensitized process which is not directly related to the real photocatalytic features of the hybrid material, the studies that use MB alone with hybrid materials and illumination with not well characterized emission could lead to misleading conclusions on the role of rGO. It is not possible to generalize the conclusions obtained on the photocatalytic behavior of the materials we synthesized to the entire set of reported TiO_2-rGO materials, because the numerous modifications of the TiO_2-rGO synthetic strategies can affect abruptly their photocatalytic performance. In particular the degree of rGO reduction can influence the energy position of its LUMO allowing/hindering the electron injection from/toward adsorbed species. Residual oxygenated groups on rGO can also be involved in acid-base equilibria which can shift the Fermi level position of rGO as a function of pH, changing the relative position of its electronic states in comparison with those of TiO_2.

Our study strongly suggests that among many mechanisms reported on the role of rGO (and graphene) the electron transfer process can occur from photoexcited states of rGO onto the titania, and holes from titania migrate to it, where adsorbed substrates are oxidized only if their HOMO has higher energy (less positive standard redox potential) than the empty state of excited rGO. Then, reduced graphene (and possibly also graphene) is advantageous when substrates are adsorbed and when the charge separation is possible (coupled with a proper semiconductor like TiO_2). Alone, or coupled with low work function oxides, rGO could be ineffective.

Acknowledgements

The authors are kindly grateful for the financial support to Regione Piemonte (ca(R)vour project - DD n.729 29/10/2014, “Piattaforme Innovative P.O.R. FESR 2007 – 2013”), Università di Torino – (Ricerca Locale) and Università di Torino & Compagnia di S.Paolo (PHOTORECARB project - Progetti di Ateneo/CSP 2012 – Call 03) and to Dr. A. Battiato for his technical support during XPS analysis.

SUPPLEMENTARY MATERIAL

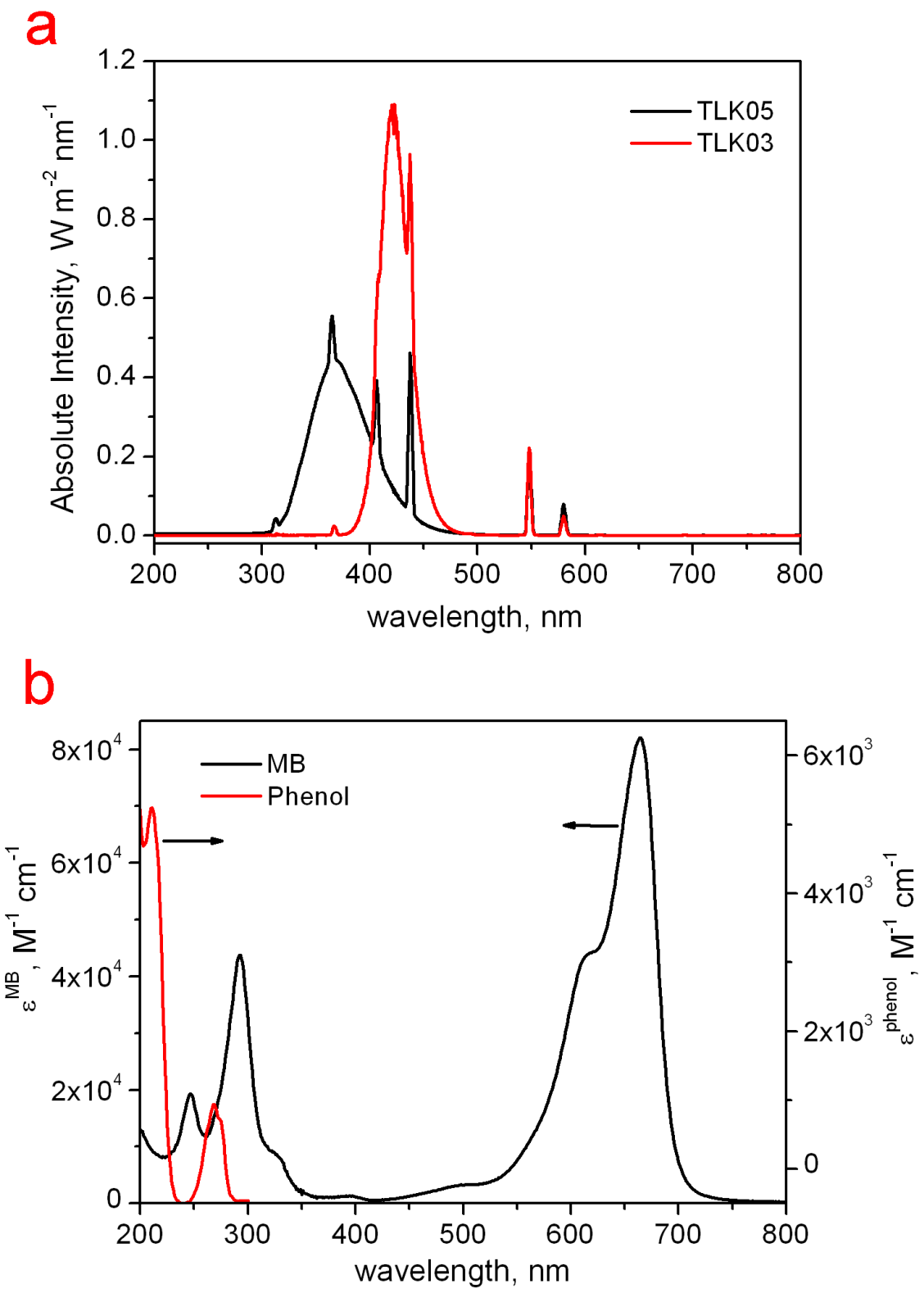

Fig. 1-SM (A) Emission spectra of the lamps adopted for the irradiation tests in the 200-800 nm range; (B) Absorption spectra of phenol and methylene blue in the 200-800 nm range.

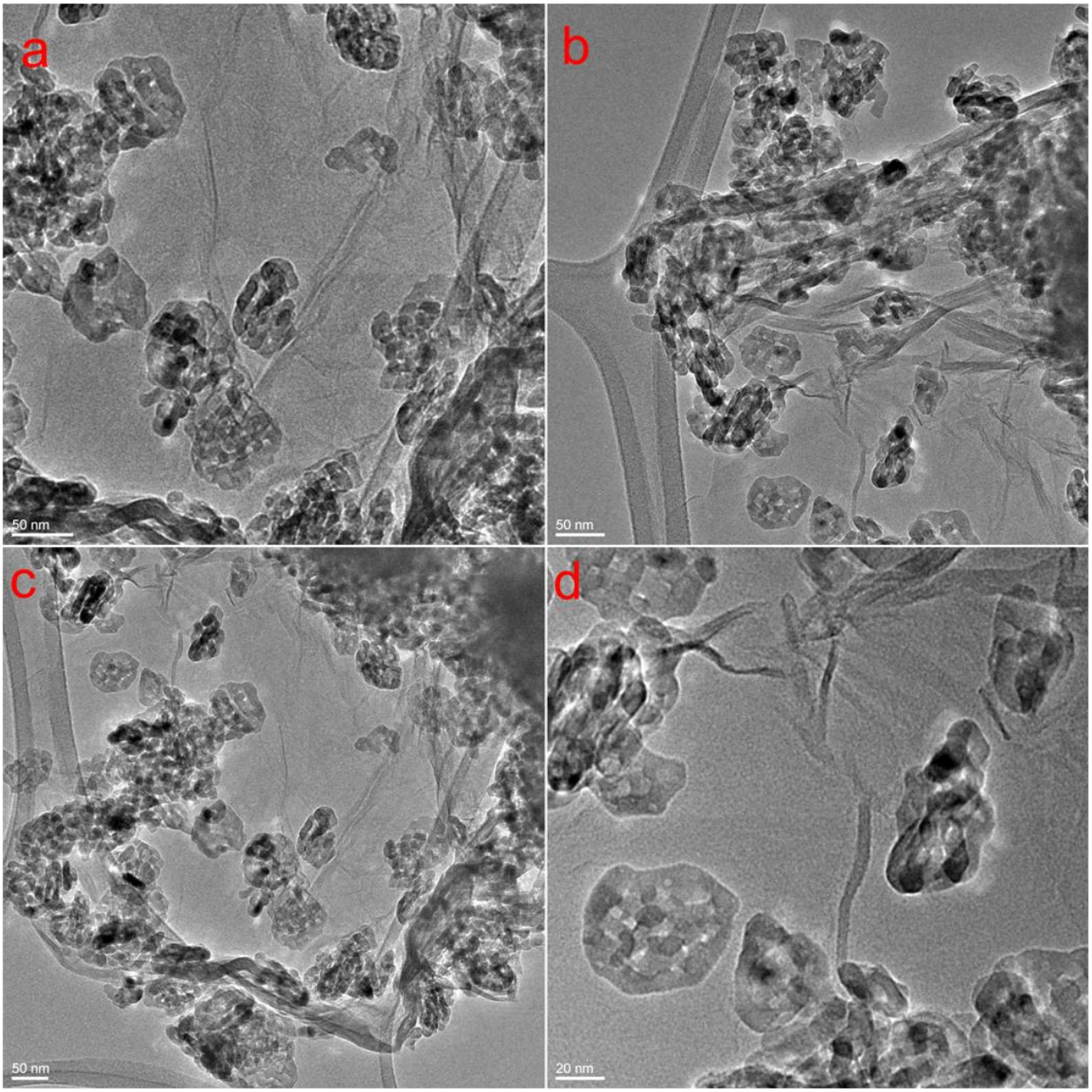

Fig. 2-SM HR-TEM micrographs of the sample TiO_2-GO before chemical reduction with 5% GO loading. Original magnifications: a) × 50 k, b) × 40 k, c) × 30 k and d) × 100 k.

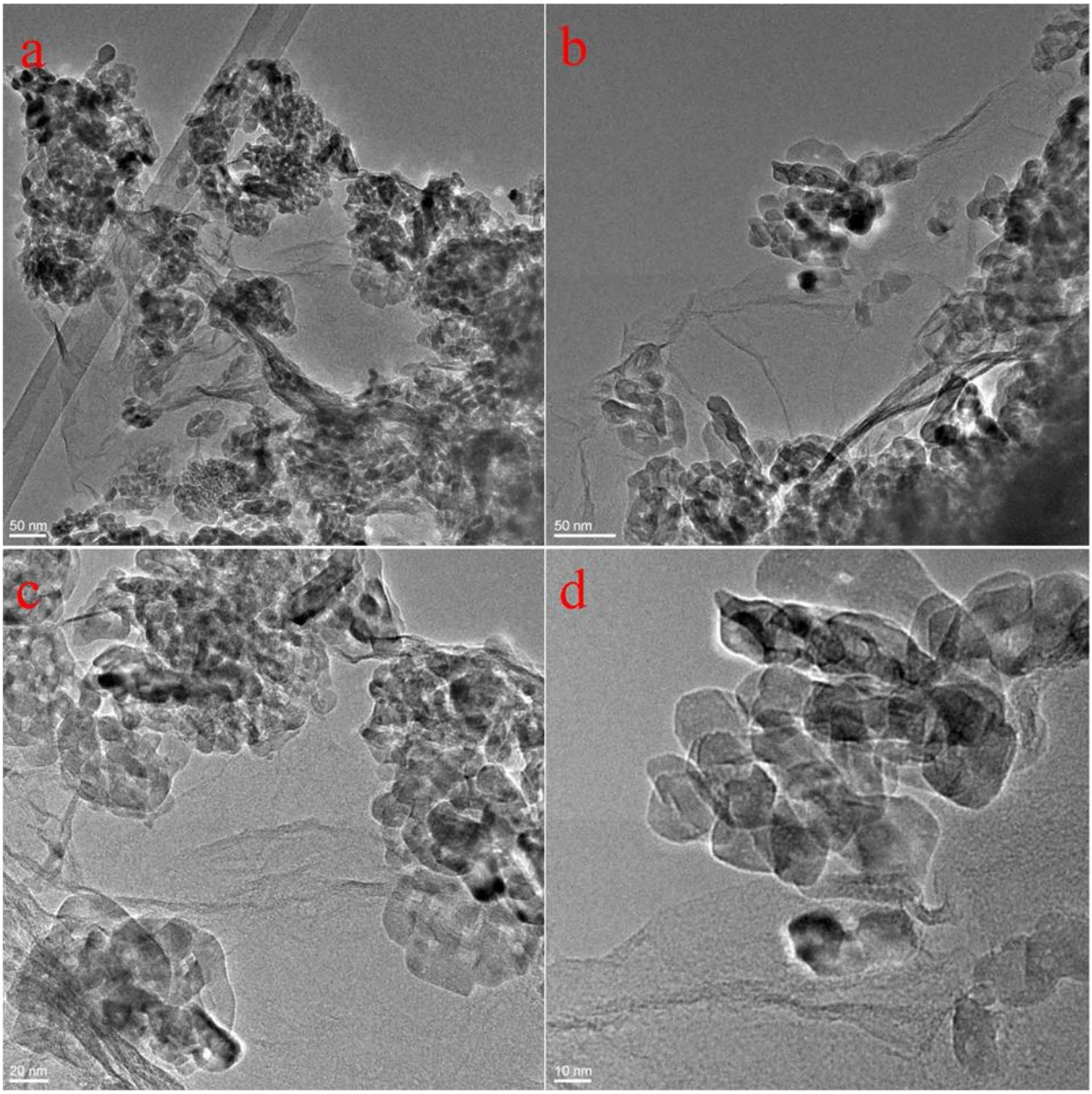

Fig. 3-SM (A) HR-TEM micrographs of the sample TiO_2-rGO with 5% rGO loading. Original magnifications: a) × 30 k, b) × 40 k, c) × 100 k and d) × 200 k.

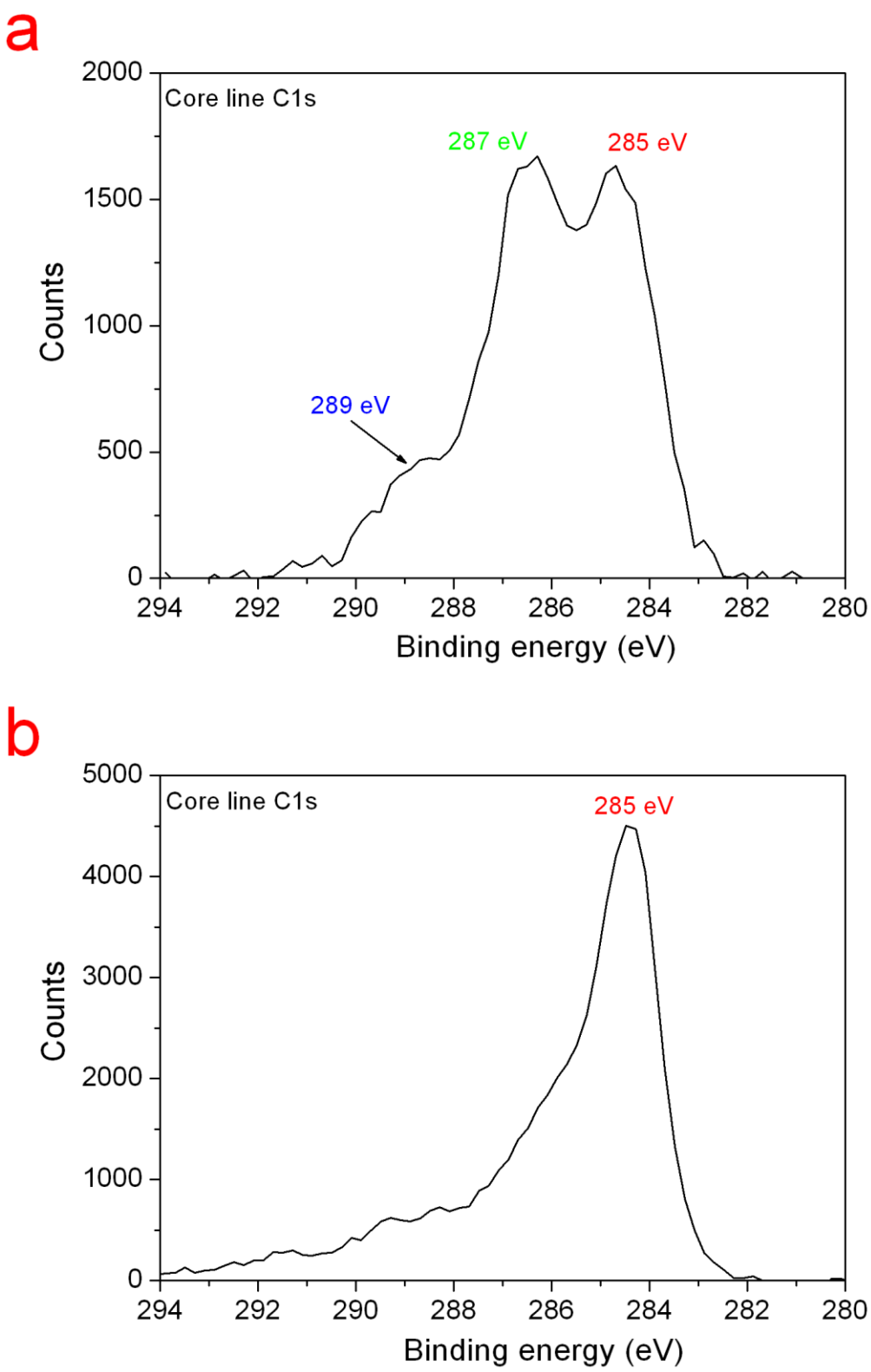

Fig. 4-SM. XPS-ESCA peak of C(1s) core level of a) TiO_2- GO, b) TiO_2-rGO(chem), with a 5% GO/rGO loading.

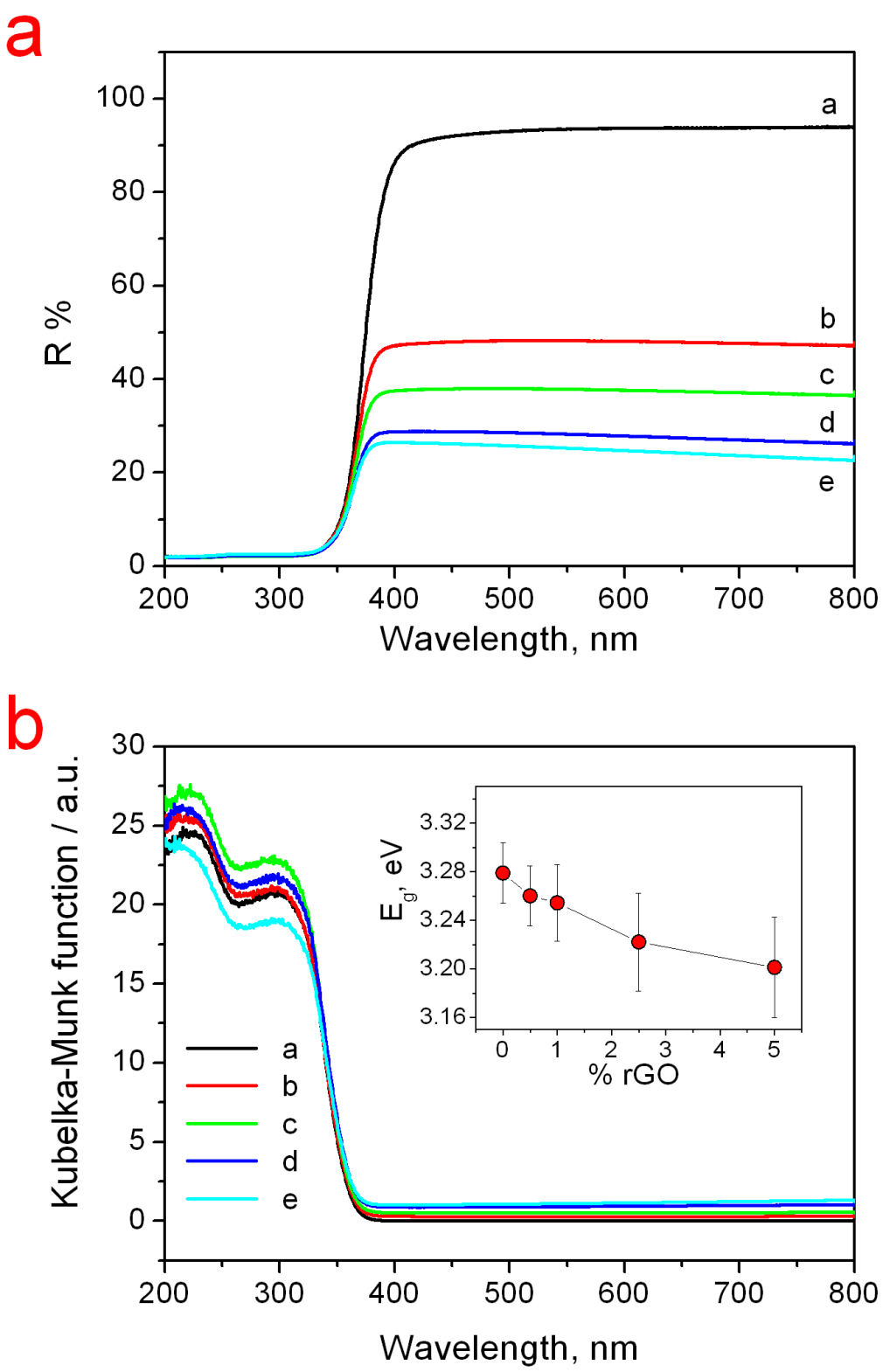

Fig. 5-SM Diffuse reflectance spectra of TiO_2-rGO hybrid materials at different rGO loadings: a = 0, b = 0.5, c = 1, d = 2.5 and e = 5 %; A) Spectra in % Reflectance; B) Spectra in Kubelka-Munk function (inset: apparent bang gap as a function of the % rGO.

608 **Table 1-SM** Pseudo first-order kinetic constants with the related error for all the photocatalytic
609 transformation of phenol and MB under irradiated (UV-Vis and Vis only)
610

Entry	Substrate	Irradiation	%rGO	k, min^{-1}
1	Phenol	UV-Vis	0	$(4.91\pm0.09)\times10^{-3}$
2	Phenol	UV-Vis	0.5	$(4.0\pm0.1)\times10^{-3}$
3	Phenol	UV-Vis	1	$(3.8\pm0.1)\times10^{-3}$
4	Phenol	UV-Vis	2.5	$(3.20\pm0.07)\times10^{-3}$
5	Phenol	UV-Vis	5	$(2.36\pm0.06)\times10^{-3}$
6	MB	UV-Vis	0	$(3.8\pm0.4)\times10^{-2}$
7	MB	UV-Vis	1	$(2.0\pm0.2)\times10^{-2}$
8	MB	UV-Vis	2.5	$(1.6\pm0.1)\times10^{-2}$
9	MB	UV-Vis	5	$(4.0\pm0.4)\times10^{-2}$
10	MB	Vis only	0	$(1.6\pm0.1)\times10^{-3}$
11	MB	Vis only	1	$(1.29\pm0.05)\times10^{-3}$
12	MB	Vis only	2.5	$(1.75\pm0.12)\times10^{-3}$
13	MB	Vis only	5	$(2.6\pm0.1)\times10^{-3}$

611
612
613
614

615 ***References***

[1] M.R. Hoffman, S.T. Martin, W. Choi, D.W. Bahnemann, Chem. Rev. 95 (1995) 69-96.
[2] T.L. Thompson, J.T. Yates, Chem. Rev. 106 (2006) 4428-4453.
[3] C. Minero, V. Maurino, E. Pelizzetti, Mechanism of the Photocatalytic Transformation of Organic Compounds, in: V. Ramamurthy, K.S. Schanze (Eds.), Semiconductor Photochemistry and Photophysics (Molecular and Supramolecular Photochemistry, Vol. 10), Marcel Dekker, New York, 2003, pp. 211-229.
[4] R. Wang, K. Hashimoto, A. Fujishima, Nature 388 (1997) 431-432.
[5] B. O'Regan, M. Grätzel, Nature 353 (1991) 737-739.
[6] V. Maurino, A. Bedini, M. Minella, F. Rubertelli, E. Pelizzetti, C. Minero, J. Adv. Oxid. Technol. 11 (2008) 184-192.
[7] C. Minero, Catal. Today 54 (1999) 205-216.
[8] J.C. Yu, J. Yu, W. Ho, Z. Jiang, L. Zhang, Chem. Mater. 14 (2002) 3808-3816.
[9] G. Barolo, S. Livraghi, M. Chiesa, M.C. Paganini, E. Giamello, J. Phys. Chem. C 116 (2012) 20887-20894.
[10] G. Yang, Z. Yan, T. Xiao, Appl. Surf. Sci. 258 (2012) 8704-8712.
[11] Y. Shiraishi, D. Tsukamoto, Y. Sugano, A. Shiro, S. Ichikawa, S. Tanaka, T. Hirai, ACS Catal. 2 (2012) 1984-1992.
[12] F. Sordello, C. Duca, V. Maurino, C. Minero, Chem. Commun. 47 (2011) 6147-6149.
[13] F. Sordello, V. Maurino, C. Minero, J. Mater. Chem. 21 (2011) 19144-19152.
[14] S. Lou, X. Guo, T. Fan, D. Zhang, Energy Environ. Sci. 5 (2012) 9195-9216.
[15] F. Sordello, C. Minero, Appl. Catal. B: Environ. 163 (2015) 452-458.
[16] C. Minero, G. Mariella, V. Maurino, E. Pelizzetti, Langmuir 16 (2000) 2632-2641.
[17] M. Minella, M.G. Faga, V. Maurino, C. Minero, E. Pelizzetti, S. Coluccia, G. Martra, Langmuir 26 (2010) 2521-2527.
[18] N. Zhang, Y. Zhang, Y.-J. Xu, Nanoscale 4 (2012) 5792-5813.
[19] V.R. Djokić, A.D. Marinković, M. Mitrić, P.S. Uskoković, R.D. Petrović, V.R. Radmilović, D.T. Janaćković, Ceram. Int. 38 (2012) 6123-6129.
[20] S. Battiston, M. Minella, R. Gerbasi, F. Visentin, P. Guerriero, A. Leto, G. Pezzotti, E. Miorin, M. Fabrizio, C. Pagura, Carbon 48 (2010) 2470-2477.
[21] L.-L. Tan, S.-P. Chai, A.R. Mohamed, ChemSusChem 5 (2012) 1868-1882, and references therein.
[22] K.S. Novoselov, A.K. Geim, S.V. Morozov, D. Jiang, Y. Zhang, S.V. Dubonos, I.V. Grigorieva, A.A. Firsov, Science 306 (2004) 666-669.
[23] J.N. Coleman, M. Lotya, A. O'Neill, S.D. Bergin, P.J. King, U. Khan, K. Young, A. Gaucher, S. De, R.J. Smith, I.V. Shvets, S.K. Arora, G. Stanton, H.-Y. Kim, K. Lee, G.T. Kim, G.S. Duesberg, T. Hallam, J.J. Boland, J.J. Wang, J.F. Donegan1, J.C. Grunlan, G. Moriarty, A. Shmeliov, R.J. Nicholls, J.M. Perkins, E.M. Grieveson, K. Theuwissen, D.W. McComb, P.D. Nellist, V. Nicolosi, Science 331 (2011) 568-571.
[24] C. Berger, Z. Song, X. Li, X. Wu, N. Brown, C. Naud, D. Mayou, T. Li, J. Hass, A.N. Marchenkov, E.H. Conrad, P.N. First, W.A. de Heer, Science 312 (2006) 1191-1196.
[25] M. Peplow, Nature 503 (2013) 327-329.
[26] L. Anfossi, P. Calza, F. Sordello, C. Giovannoli, F. Di Nardo, C. Passini, M. Cerruti, I.Y. Goryacheva, E.S. Speranskaya, C. Baggiani, Anal. Bioanal. Chem. 406 (2014) 4841-4849.
[27] F. Sordello, G. Zeb, K. Hu, P. Calza, C. Minero, T. Szkopekc, M. Cerruti, Nanoscale, 6 (2014) 6710-6719.
[28] T. Szabó, O. Berkesi, P. Forgó, K. Josepovits, Y. Sanakis, D. Petridis, I. Dékány, Chem. Mater. 18 (2006) 2740-2749.
[29] M. Minella, M. Demontis, M. Sarro, F. Sordello, P. Calza, C. Minero, J. Mater. Sci. 50 (2015) 2399-2409.

[30] L.M. Pastrana-Martínez, S. Morales-Torres, V. Likodimos, J.L. Figueiredo, J.L. Faria, P. Falaras, A.M.T. Silva, Appl. Catal. B: Environ. 123-124 (2012) 241-256.
[31] Y. Wang, R. Shi, J. Lin, Y. Zhu, Appl. Catal. B: Environ. 100 (2010) 179-183.
[32] R. Long, N.J. English, O.V. Prezhdo, J. Am. Chem. Soc. 134 (2012) 14238-14248.
[33] Y. Zhang, N. Zhang, Z.-R. Tang, Y.-L. Xu, ACS Nano 6 (2012) 9777-9789.
[34] G. Williams, B. Seger, P.V. Kamat, ACS Nano 2 (2008) 1487-1491.
[35] I.V. Lightcap, T.H. Kosel, P.V. Kamat, Nano Lett. 10 (2010) 577-583.
[36] J. Zhang, Z. Xiong, X.S. Zhao, J. Mater. Chem. 21 (2011) 3634-3640.
[37] P. Wang, J. Wang, X. Wang, H. Yu, J. Yu, M. Lei, Y. Wang, Appl. Catal. B: Environ. 132-133 (2013) 452-459.
[38] E. Pelizzetti, V. Maurino, C. Minero, V. Carlin, E. Pramauro, O. Zerbinati, Environ Sci Technol 24 (1990) 1559-1565.
[39] V. Maurino, M. Minella, F. Sordello, C. Minero, Appl. Catal. A: Gen. (2015) http://dx.doi.org/10.1016/j.apcata.2015.11.012.
[40] W.S. Hummers, R.E. Offeman, J. Am. Chem. Soc. 80 (1958) 1339.
[41] N.M. Huang, H.N. Lim, C.H. Chia, M.A. Yarmo, M.R. Muhamad, Int. J. Nanomed. 6 (2011) 3443-3448.
[42] W. Fan, Q. Lai, Q. Zhang, Y. Wang. J. Phys. Chem. C 115 (2011) 10694-10701.
[43] V. Pagonis, C. Ankjærgaard, A.S. Murray, R. Chen, J. Lumin. 129 (2009) 1003-1009.
[44] M. Lotya, Y. Hernandez, P.J. King, R.J. Smith, V. Nicolosi, L.S. Karlsson, F.M. Blighe, S. De, Z. Wang, I.T. McGovern, G.S. Duesberg, J.N. Coleman, J. Am. Chem. Soc. 131 (2009) 3611-3620.
[45] A.B. Bourlinos, V. Georgakilas, R. Zboril, T.A. Steriotis, A.K. Stubos, C. Trapalis, Solid State Commun. 149 (2009) 2172-2176.
[46] Q. Mei, K. Zhang, G. Guan, B. Liu, S. Wang, Z. Zhang, Chem. Commun. 46 (2010) 7319-7321.
[47] D. Li, M.B. Mueller, S. Gilje, R.B. Kaner, G.G. Wallace, Nat. Nanotechnol. 3 (2008) 101-105.
[48] D.C. Marcano, D.V. Kosynkin, J.M. Berlin, A. Sinitskii, Z. Sun, A. Slesarev, L.B. Alemany, W. Lu, J.M. Tour, ACS Nano 4 (2010) 4806-4814.
[49] X. Gao, J. Jang, S. Nagase, J. Phys. Chem. C 114 (2010) 832-842.
[50] N. M. Huang, H. N. Lim, C. H. Chia, M. A. Yarmo, M. R. Muhamad, Int. J. Nanomed. 6 (2011) 3443-3448.
[51] S. Pei, H.-M. Cheng, Carbon 50 (2012) 3210-3228
[52] M. Bruna, B. Massessi, C. Cassiago, A. Battiato, E. Vittone, G. Speranza, S. Borini, J. Mater. Chem. 51 (2011) 18730-18737.
[53] J. Shang, L. Ma, J. Li, W. Ai, T. Yu, G.G. Gurzadyan, Sci. Rep. 2 (2012) 792, DOI: 10.1038/srep00792.
[54] Y. Zhang, Z.-R. Tang, X. Fu, Y.-J. Xu, ACS Nano 4 (2010) 7303-7314.
[55] H. Zhang, X. Lv, Y. Li, Y. Wang, J. Li, ACS Nano 4 (2010) 380-386.
[56] V. Štengl, D. Popelková, P. Vláčil, J. Phys. Chem. C 115 (2011) 25209-25218.
[57] K. Woan, G. Pyrgiotakis, W. Sigmund, Adv. Mater. 21 (2009) 2233-2239.
[58] M.S.A.S. Shah, A.R. Park, K. Zhang, J.H. Park, P.J. Yoo, Appl. Mater. Interfaces 4 (2012) 3893-3901.
[59] B. El-Kareh, Fundamentals of Semiconductor Processing Technologies, Kluwer Academic Publishers, Norwell, 1995.
[60] M. Liška, Ľ. BartoŠ, J. Valášek, Chem. Papers 43 (1989) 303-313, and references therein.
[61] K. Patil, R. Pawar, P. Talap, Phys. Chem. Chem. Phys. 2 (2000) 4313-4317.
[62] A. Ghanadzadeh , A. Zeini, A. Kashef, M. Moghadam, J. Mol. Liq. 138 (2008) 100-106.
[63] T. Xiong, F. Dong, Y. Zhou, M. Fu, W.-K. Ho, J. Colloid. Interface Sci. 447 (2015) 16-24.

[64] P. Calza, C. Hadjicostas, V.A. Sakkas, M. Sarro, C. Minero, C. Medana, T.A. Albanis, Appl. Catal. B: Environ. 183 (2016) 96-106.
[65] N. Martsinovich, A. Troisi, Phys. Chem. Chem. Phys. 14 (2012) 13392-13401.
[66] R. Abe, K. Sayama, H. Arakawa, J. Photochem. Photobiol., A 166 (2004) 115-122.
[67] M.-Q. Yang, Y.-J. Xu, J. Phys. Chem. C 117 (2013) 21724−21734.